AGU PUBLICATIONS

Water Resources Research

RESEARCH ARTICLE
10.1002/2014WR016017

Key Points:
- We compare coupled and uncoupled hydrogeophysical inversions based on EnKF
- The coupled approach outperforms the uncoupled if prior statistics are correct
- The uncoupled approach is less affected by filter inbreeding than the coupled

Correspondence to:
M. Camporese,
matteo.camporese@unipd.it

Citation:
Camporese, M., G. Cassiani, R. Deiana, P. Salandin, and A. Binley (2015), Coupled and uncoupled hydrogeophysical inversions using ensemble Kalman filter assimilation of ERT-monitored tracer test data, *Water Resour. Res.*, *51*, 3277–3291, doi:10.1002/2014WR016017.

Received 18 JUN 2014
Accepted 4 APR 2015
Accepted article online 8 APR 2015
Published online 8 MAY 2015

Coupled and uncoupled hydrogeophysical inversions using ensemble Kalman filter assimilation of ERT-monitored tracer test data

Matteo Camporese[1], Giorgio Cassiani[2], Rita Deiana[3], Paolo Salandin[1], and Andrew Binley[4]

[1]Department of Civil, Environmental and Architectural Engineering, University of Padua, Padua, Italy, [2]Department of Geosciences, University of Padua, Padua, Italy, [3]Department of Cultural Heritage: Archaeology and History of Art, Cinema and Music, University of Padua, Padua, Italy, [4]Lancaster Environment Centre, Lancaster University, Lancaster, UK

Abstract Recent advances in geophysical methods have been increasingly exploited as inverse modeling tools in groundwater hydrology. In particular, several attempts to constrain the hydrogeophysical inverse problem to reduce inversion errors have been made using time-lapse geophysical measurements through both coupled and uncoupled (also known as sequential) inversion approaches. Despite the appeal and popularity of coupled inversion approaches, their superiority over uncoupled methods has not been proved conclusively; the goal of this work is to provide an objective comparison between the two approaches within a specific inversion modeling framework based on the ensemble Kalman filter (EnKF). Using EnKF and a model of Lagrangian transport, we compare the performance of a fully coupled and uncoupled inversion method for the reconstruction of heterogeneous saturated hydraulic conductivity fields through the assimilation of ERT-monitored tracer test data. The two inversion approaches are tested in a number of different scenarios, including isotropic and anisotropic synthetic aquifers, where we change the geostatistical parameters used to generate the prior ensemble of hydraulic conductivity fields. Our results show that the coupled approach outperforms the uncoupled when the prior statistics are close to the ones used to generate the true field. Otherwise, the coupled approach is heavily affected by "filter inbreeding" (an undesired effect of variance underestimation typical of EnKF), while the uncoupled approach is more robust, being able to correct biased prior information, thanks to its capability of capturing the solute travel times even in presence of inversion artifacts such as the violation of mass balance. Furthermore, the coupled approach is more computationally intensive than the uncoupled, due to the much larger number of forward runs required by the electrical model. Overall, we conclude that the relative merit of the coupled versus the uncoupled approach cannot be assumed a priori and should be assessed case by case.

1. Introduction

Hydrological models often require abundant and high-quality data in order to deliver reliable results and predictions. While this has been known for a long time, only the availability of (a) novel data and (b) more advanced methods to exploit the data information has recently fostered our capability of building better models that have a conceptual structure consistent with reality and reproduce more accurately all available data.

Concerning new data availability, the use of geophysical data for hydrological purposes has had a tremendous impulse in the 1990s, as the mutual understanding of hydrological needs and geophysical potential matured in the two scientific communities. This ultimately led to the development of a discipline of its own, named hydrogeophysics, i.e., the investigation through minimally invasive techniques of the shallow subsurface, with the aim of understanding its hydrological properties. This is now a very active field of research [e.g., *Vereecken et al*., 2006; *Singha et al*., 2015], with a number of studies recently appeared in the literature, emphasizing particularly on ground-penetrating radar (GPR) [e.g., *Annan*, 2005] and electrical resistance tomography (ERT) [e.g., *Binley and Kemna*, 2005]. These techniques work not only as powerful imaging methods but also as means to measure changes in soil moisture content [e.g., *Deiana et al*., 2008] or solute concentration [e.g., *Cassiani et al*., 2006] by conducting time-lapse measurements. While a number of issues are still open regarding the resolution characteristics of each geophysical method, hydrogeophysical

investigations have received wider acceptance in the hydrological community. A strength of these techniques lies in the possibility of deriving, albeit often approximately, estimates of hydrological state variables (such as solute concentration or water saturation) at the spatial and temporal scale, depth, and resolution needed in hydrological sciences, and often not achievable with traditional monitoring techniques [*Singha et al*., 2015]. However, it is well known that resolution limitations [*Day-Lewis et al*., 2005] can produce severe mass balance errors [*Singha and Gorelick*, 2005] even in the most favorable cross-hole configurations. The problem can be even more serious when surface-based ERT is used to monitor natural or artificial irrigation from the ground surface [e.g., *Cassiani et al*., 2012], where resolution dramatically drops with depth and a direct conversion of inverted resistivity values into estimates of soil moisture content may prove elusive.

Conversely, the traditional use of data to calibrate hydrological models has made tremendous progresses in the past two decades, partly thanks to the ever increasing available computational power. Many inverse models have been developed to estimate aquifer hydraulic properties [e.g., *Carrera and Neuman*, 1986; *Certes and De Marsily*, 1991; *Carrera et al*., 1993; *RamaRao et al*., 1995; *McLaughlin and Townley*, 1996; *Gomez-Hernandez et al*., 1997; *Zimmerman et al*., 1998; *Vrugt et al*., 2008; *Hendricks and Kinzelbach*, 2009; *Zhou et al*., 2014], where, traditionally, hydraulic conductivity and head measurements have been used to provide the necessary information [e.g., *Chen and Zhang*, 2006; *Hendricks Franssen and Kinzelbach*, 2008; *Karahan and Ayvaz*, 2008; *Li et al*., 2012; *Xu et al*., 2013]. Alternative techniques that have recently gained interest in this framework are data assimilation schemes (see *Judd and Stemler* [2010] and *Montzka et al*. [2012] for recent discussions on this topic), which allow automatic incorporation of measured information into numerical simulations. While the parameter estimation problem is different from the state estimation problem, the two can be combined in data assimilation, where an improved state estimate and a set of improved model parameters are searched for simultaneously [*Evensen*, 2009]. In addition to being able to solve the inverse problem, these techniques are developed with the aim of preserving the dynamics of the system, and for this reason are of high interest in hydrological modeling [e.g., *Pauwels et al*., 2001; *Margulis et al*., 2002]. Ensemble Kalman filter (EnKF) and its variations (e.g., ensemble smoother) are particularly well suited for our types of applications [e.g., *Camporese et al*., 2009a, 2009b, 2011; *Crestani et al*., 2013], thanks to their capability to solve efficiently the combined parameter and state estimation problem [*Evensen*, 2009].

Geophysical measurements can be informative of the hydrological response of the soil and groundwater if applied in time-lapse monitoring mode. In particular, many authors have recently demonstrated that it is possible to use geophysical methods to effectively monitor a saline tracer that moves within the subsurface and, from that knowledge, to infer the spatial variability of hydraulic parameters, in particular the hydraulic conductivity [*Kemna et al*., 2002; *Irving and Singha*, 2010; *Pollock and Cirpka*, 2010; *Camporese et al*., 2011]. However, in order to extract this hydrological information, the assimilation of measurements in a hydrological model is needed. Two different approaches may be applied, named respectively, "uncoupled" (or "sequential") and "coupled" hydro-geophysical inversions.

The procedure for an uncoupled inversion can be summarized by the following steps:

1. The spatial distribution of the geophysical quantity of interest (e.g., electrical resistivity for ERT) is derived from the inversion of geophysical field data.
2. The application of a petrophysical relationship leads to obtaining, from the geophysical quantity, an estimation of moisture content or concentration distribution.
3. The estimated hydrologic state variable (concentration or moisture content), in its spatiotemporal distribution, is used to calibrate and constrain a hydrological model, thus identifying the corresponding governing parameters (e.g., hydraulic conductivity).

The inversion of geophysical measurements is usually a problem characterized by ill-posedness, which can be tackled using prior information. If no solid independent information is available, the most common approach is the introduction of a regularizing functional, commonly a smoothness constraint [e.g., *Menke*, 1984]. As a consequence of ill-posedness and regularization, the inversion procedure can lead to artifacts, misinterpretations, and unphysical results, especially in the subsurface regions where the sensitivity of the measurements is low [e.g., *Day-Lewis et al*., 2005].

To overcome these problems, a coupled hydrogeophysical modeling can be applied [e.g., *Busch et al*., 2013; *Jardani et al*., 2013; *Soueid Ahmed et al*., 2014; *Tran et al*., 2014], consisting typically of the following steps:

1. A hydrological model is used to predict the evolution of hydrological state variables, e.g., moisture content or concentration, on the basis of a set of hydrological governing parameters, the identification of which is the final aim of the inversion.
2. A suitable petrophysical relationship (same as for point (2) above) translates hydrological state variables into geophysical quantities, such as resistivity or dielectric constant.
3. The simulated geophysical quantities are used to predict the geophysical field measurements.
4. A comparison between predicted and measured geophysical (and hydrological, when available) field measurements allows a calibration of the complex of hydrological and geophysical models (thus the definition "coupled inversion"), leading to the identification of the hydrological parameters, which are the key objective of the study.

Although it is commonly believed that fully coupled approaches are superior to the uncoupled ones, very few studies comparing the two approaches in a comprehensive and objective manner are available in the literature [e.g., *Hinnell et al*., 2010]. Due to the increasing interest in the use of data assimilation techniques as inversion tools, the main goal of this paper is to compare the coupled and uncoupled versions of a specific inverse modeling framework, based on the Lagrangian formulation of transport and the ensemble Kalman filter (EnKF). The inversion model is here applied to assess the spatial distribution of hydraulic conductivity (K) by assimilating time-lapse cross-hole electrical resistivity tomography (ERT) data generated for a synthetic tracer test in a heterogeneous aquifer. In the coupled approach, the K distribution is retrieved by assimilating raw ERT resistance data without a preliminary geoelectrical inversion. In the uncoupled approach, K is estimated by assimilating electrical conductivity data derived from a previously performed traditional geophysical inversion of the same resistance data set. We compare the performance of the two approaches in a number of simulation scenarios, both isotropic and anisotropic, each of them characterized by a different choice of the geostatistical parameters used to generate the prior ensemble of K distributions.

2. Theory and Methods

2.1. Flow and Transport Model

The problem of nonreactive transport in a two-dimensional heterogeneous flow field is solved here via the Lagrangian approach [*Dagan*, 1989], following the method proposed by *Salandin and Fiorotto* [1998]. First, the steady state flow field in a saturated, spatially heterogeneous porous medium is computed by solving the equation

$$\nabla \cdot (K \nabla H) = 0, \tag{1}$$

defined over a domain Ω with prescribed conditions on the boundary Γ. In equation (1), K is saturated hydraulic conductivity, H is hydraulic head, and ∇ is the gradient operator.

The hydraulic conductivity field $K(\mathbf{x})$ is assumed, as usual, lognormally distributed, and characterized by the mean value $\langle Y \rangle$ and the covariance structure $C_Y(r) = \sigma_Y^2 exp(-r/I_r)$, where $Y = \log K$ is the hydraulic log- conductivity, r is the separation distance measured either along the coordinate x or z, I_r is the relevant integral scale (I_x or I_z, according to the coordinate), and σ_Y^2 is the hydraulic log-conductivity variance [*Dagan*, 1989].

Equation (1) is solved using bilinear finite elements in order to compute the spatial distribution of H (piezometric field). A continuous Eulerian velocity field $\mathbf{V}(\mathbf{x})$ is obtained adopting the method proposed by *Cordes and Kinzelbach* [1992], according to whom the velocity field is given from a known distribution of hydraulic head by subdividing each quadrilateral element into four subelements. A continuous flux distribution across the boundaries of the subelements is computed by imposing conditions of continuity and irrotationality. The stream function is interpolated over each subelement using the same bilinear shape function used for the piezometric field.

The integral relationship between the resulting continuous flow field and the Lagrangian trajectory of the solute particle $\mathbf{X}_t(\mathbf{x}_0, t)$ is

$$\mathbf{X}_t(\mathbf{x}_0, t) = \int_0^t \mathbf{V}(\mathbf{X}_\tau(\mathbf{x}_0, \tau))d\tau, \tag{2}$$

where $\mathbf{x}_0$ is the particle coordinate at the starting point at $t = 0$. In our simulations we assume Lagrangian stationarity and neglect pore-scale dispersion and diffusion, the transport process being dominated by the spatial variability of K at larger scales [*Dagan*, 1989].

Within this framework, the continuously distributed injection of a nonreactive solute in an area A_0 can be approximated by the release of a large finite set of N particles regularly spaced at intervals $\Delta\mathbf{x}_0$. A dimensionless measure of the solute concentration C over a finite element of area ΔA ($\gg \Delta\mathbf{x}_0$) and centroid located in $\mathbf{x}$ is given by [*Camporese et al.*, 2011; *Crestani et al.*, 2013]

$$\begin{aligned} C(\mathbf{x}, t; t_0) &= \frac{\phi}{M}\int_{\Delta A}\int_{A_0} C_0(\mathbf{x}_0)\delta[\mathbf{x}' - \mathbf{X}_t(\mathbf{x}_0, t_0)]d\mathbf{x}_0\, d\mathbf{x}' \\ &= \frac{1}{N\Delta A}\int_{\Delta A}\sum_{i=1}^{N}\delta[\mathbf{x}' - \mathbf{X}_t(\mathbf{x}_0, t_0)]\Delta\mathbf{x}_0\, d\mathbf{x}', \end{aligned} \tag{3}$$

where $M = \phi C_0 A_0$ is the total mass of initial concentration C_0 uniformly injected in the area A_0, being ϕ the porosity, and δ is the Dirac delta function. In this study, we consider the spatial variability of ϕ negligible with respect to that of K, as usually assumed in natural sedimentary aquifers [*Gelhar*, 1993].

2.2. Electrical Model

The relationship between the electrical properties of a porous medium, its structural characteristics, and its hydrological state is generally defined by empirical laws. In this paper, we adopted the well-known Archie's law [*Archie*, 1942], where any effect of surface electrical conductivity is neglected, and bulk electrical conductivity σ depends on water saturation S_w (always equal to 1 in this study) and pore water electrical conductivity σ_w

$$\sigma = \phi^m S_w^n \sigma_w, \tag{4}$$

where m ("cementation exponent") and n ("saturation exponent") are site-specific empirical parameters and σ_w is a function of the tracer concentration.

Electrical resistivity tomography (ERT) is an inversion technique that allows the reconstruction of the bulk electrical conductivity distribution in space, and often in time, starting from the measurements of injected current I_e and resulting voltage V_e (and thus the relevant resistance $R = V_e/I_e$) at two distinct pairs of electrodes [*Binley and Kemna*, 2005]. ERT is composed of

1. A forward model that can predict resistance values, given the space-time distribution of bulk electrical conductivity, and that is in practice a numerical solution of the partial differential equation

$$\nabla \cdot (\sigma \nabla V) = 0, \tag{5}$$

subjected to suitable boundary conditions. The variable V is the electric potential (voltage) and, as commonly accepted for geoelectrical methods, the model assumes point-like electrodes.

2. An inversion procedure seeking an electrical conductivity distribution that, using the forward model, reproduces the data to a specified level of uncertainty, usually derived from a quantitative estimate of measurement errors. This is normally accomplished by solving the inverse problem as a regularized optimization problem, where the objective function to be minimized can be expressed as a weighted sum of data misfit and a regularization term, usually constructed on the basis of a roughness matrix that is often chosen to be a numerical approximation of the second spatial derivative of the reconstructed conductivity field. The optimal weight between data misfit and regularization term is commonly made dependent on the error level in the data, and the corresponding solution is the smoothest compatible with the data within their error bounds (an Occam's type solution), as defined by *Binley and Kemna* [2005]. As described in *Camporese et al.* [2011], the objective function to be minimized can be expressed as

$$\psi(\mathbf{m}) = \psi_d(\mathbf{m}) + \alpha\psi_m(\mathbf{m}), \tag{6}$$

with ψ_d being the data misfit, defined as

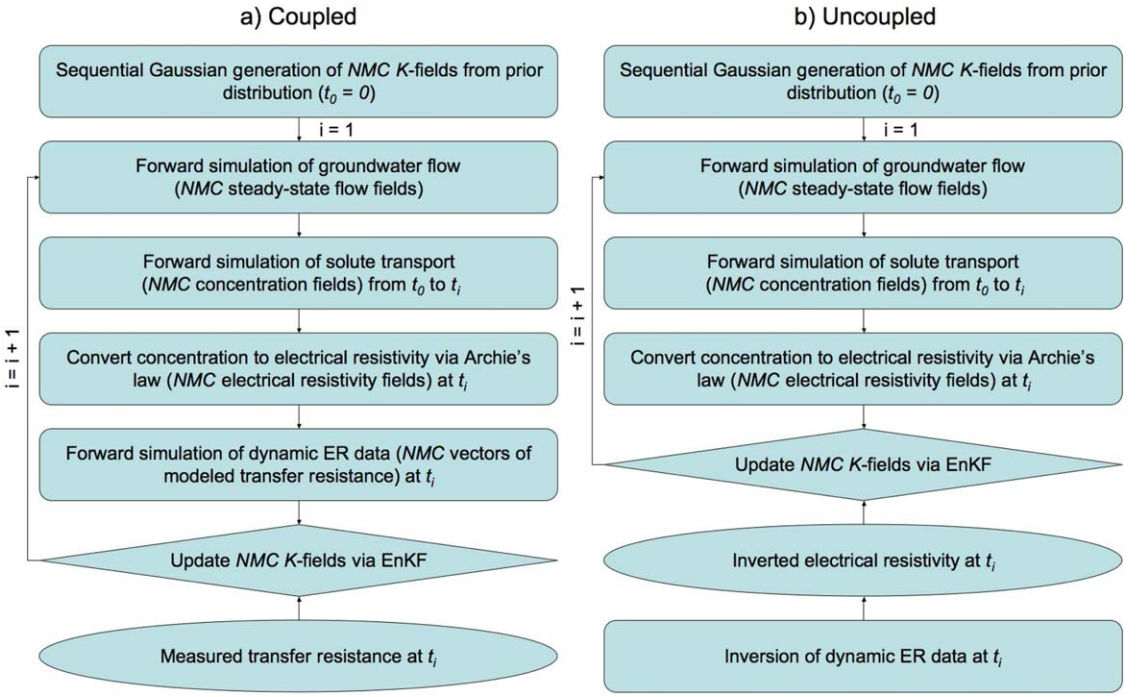

Figure 1. Flowcharts illustrating (a) the fully coupled and (b) the uncoupled inversion algorithms.

$$\psi_d(\mathbf{m}) = ||\mathbf{W}[\mathbf{d} - \mathbf{f}(\mathbf{m})]||^2, \tag{7}$$

where **m** is the vector of unknowns made of the log-transformed electrical conductivities of each grid pixel; **d** is the vector of data, made of the log-transformed electrical resistances measured at each quadrupole of electrodes; $\mathbf{f}(\mathbf{m})$ is the vector of electrical resistances predicted by the forward model derived from the numerical solution of equation (5); **W** is a data weighting matrix associated with the individual data errors; $\psi_m(\mathbf{m})$ is a regularization term taking smaller values for smoother **m** fields; and α is a regularization parameter that controls the trade-off between ψ_d and ψ_m. This inversion procedure also allows the computation of a covariance matrix of the estimated conductivity field and the corresponding measurement error covariance matrix (for details, see *Camporese et al.* [2011]).

In this work, for both forward and inverse solution of the electrical current flow problem, we used the 2-D resistivity, 3-D current ERT code R2 by A. Binley, Lancaster University (http://www.es.lancs.ac.uk/people/amb/Freeware/freeware.htm), which is based on a finite element forward model solution and on an Occam's approach to regularized inversion.

2.3. Hydrogeophysical Inversion

2.3.1. Ensemble Kalman Filter

Given a set of measurements of a system state and a dynamical model with known uncertainties, the ensemble Kalman filter (EnKF) [*Evensen*, 2009] solves the combined parameter and state estimation problem by means of a Monte Carlo approach, under the assumptions that the dynamical model is a Markov process and measurement errors are independent in time.

In this study we use the EnKF as an inversion tool to estimate the distribution of the hydraulic log-conductivity Y given a set of measurements of the solute evolution.

At time t_0, *NMC* realizations of the log-transformed hydraulic conductivity field are generated from a prior guess of the geostatistical parameters $\langle Y \rangle$, σ_Y^2, I_x, and I_z. Starting with the same initial concentration C_0 for each Y field, the solute plume is propagated forward to the first measurement time t_1, using the Lagrangian transport model described in section 2.1. At time t_1, each distribution of Y is collected in a vector $\mathbf{y}^j =$

$[Y_1, \ldots, Y_n]^j$ (where $j = 1, \ldots, NMC$ and n is the number of elements of the mesh) and updated through the equation

$$\mathbf{y}^j_{upd} = \mathbf{y}^j + \mathbf{P}_e\mathbf{H}^T(\mathbf{H}\mathbf{P}_e\mathbf{H}^T + \mathbf{R}_e)^{-1}(\mathbf{z} - \mathbf{H}\mathbf{y}^j), \quad (8)$$

where $\mathbf{y}^j_{upd}$ is the jth realization of the updated Y distribution, $\mathbf{P}_e$ is the prior estimate of the system state error covariance matrix, computed from the ensemble of realizations, $\mathbf{z}$ is the vector of observations, $\mathbf{R}_e$ is the measurement error covariance matrix, and $\mathbf{H}$ is the operator that maps model results at measurement locations to actual measurements. Here the EnKF is applied recursively, according to a scheme that is also known as restart EnKF [*Wen and Chen*, 2006; *Hendricks Franssen and Kinzelbach*, 2008; *Camporese et al*., 2011; *Crestani et al*., 2013]: (i) a propagation step, where the groundwater model is resolved from t_0 onward until new measurement data (that were not used for assimilation before) become available, followed by (ii) an update step of the log-transformed hydraulic conductivity values at each measurement time t_i. The procedure (Figure 1) is repeated until the last time t_{tm} when measurements are available. Note that update of C is not necessary, as, after each assimilation, the forward simulation is restarted, with the new Y distribution, from $t = t_0$. The update scheme adopted in this study follows the implementation described by *Sakov et al*. [2010].

The main difference between the fully coupled and the uncoupled approaches lies in the measurements assimilated, as discussed in the following sections.

2.3.2. Fully Coupled Approach

Figure 1a reports the flowchart of the fully coupled inversion approach. Starting with an ensemble of hydraulic conductivity fields generated by a standard sequential Gaussian simulator, in each field we simulate the evolution of a saline tracer by means of the Lagrangian approach described in section 2.1. Assuming that the parameters of the petrophysical relationship that links concentrations and electrical conductivities (Archie's law) are known, the distribution of σ is computed for each realization. The forward electrical model described in section 2.2 is then run for each field of electrical conductivity in order to compute the transfer resistance data forming the vectors $\mathbf{H}\mathbf{y}^j$ in equation (8), while $\mathbf{z}$ contains the resistance data measured in a reference synthetic experiment.

In the coupled approach, the matrix $\mathbf{R}_e$ is diagonal, i.e., we assume that the resistance measurement errors are independent from each other. Therefore, off-diagonal elements are set to zero, while the diagonal elements are computed by assigning a desired level of error to the measurements.

2.3.3. Uncoupled Approach

Figure 1b reports the flowchart of the uncoupled inversion approach. The algorithm follows the same steps as the fully coupled approach until the computation of the electrical conductivity fields, but in the uncoupled approach an electrical inversion is performed before running the hydrological inverse model, so that in the EnKF the vectors $\mathbf{H}\mathbf{y}^j$ contain the simulated electrical conductivities, while $\mathbf{z}^j$ is formed by the σ distributions derived from the inversion.

The matrix $\mathbf{R}_e$, in this case, is calculated through the procedure mentioned in section 2.2 and described with more details in *Camporese et al*. [2011]. This has two main implications: first, the uncertainty assigned to the measurements is typically much larger than the one assigned in the coupled case to the raw resistance data, because the latter are not affected by the electrical inversion; second, the off-diagonal elements are now different from zero, as the errors on the inverted σ data are not independent from each other.

3. Numerical Experiments

3.1. Setup of the Reference Scenarios

Two reference scenarios are considered, both consisting of a two-dimensional vertical cross section of an aquifer with dimensions 30×15 m^2, discretized into $60 \times 30 = 1800$ square elements of side 0.5 m. Boundary conditions consist of hydraulic head imposed (Dirichlet) at $x = 0$ m ($H = 100$ m) and at $x = 30$ m ($H = 99$ m), resulting in a mean gradient of 3.3% along the main flow direction. No flow boundary conditions (Neumann) are imposed along the upper and lower sides of the domain. Both reference hydraulic log-conductivity (Y) fields were generated using a fast Fourier transform method [*Gutjahr et al*., 1997] with mean $\langle Y \rangle = 0.0$ log(m/h) (corresponding to a geometric mean of the saturated hydraulic conductivity equal

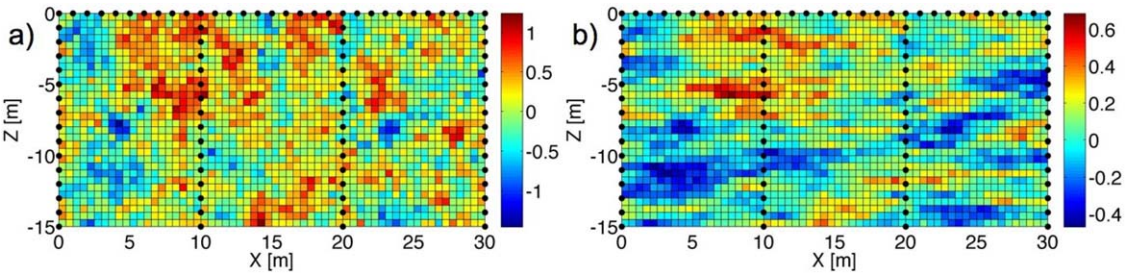

Figure 2. Reference distribution of hydraulic conductivity in the synthetic (a) isotropic and (b) anisotropic aquifers, with electrodes indicated by black dots. The color bar indicates hydraulic log-conductivity in $\log_{10}$[m/h].

to $K_G = 1.0$ m/h) and variance $\sigma_Y^2 = 1.0$ $\log^2$ (m/h). The first reference field has an isotropic exponential correlation structure with integral scale $I_x = I_z = 1.0$ m, while the second is characterized by an anisotropic exponential correlation structure with $I_x = 4.0$ m and $I_z = 1.0$ m (Figure 2).

In both cases, a slug of saline tracer is assumed to be instantaneously and uniformly injected in a source area of dimensions 1.25×11.00 m^2 (centered at $x = 1.625$ m and from $z = 2.0$ m to $z = 13.00$ m). This may represent a stylized injection well partially screened in a confined aquifer; even though the conceptualization lacks the complexities related to a real well injection (such as density effects, three-dimensionality, and skin effects), it is ideal for the purpose of comparing the two inversion approaches in a perfectly controlled setting. The injection is simulated by 2112 particles, corresponding to a density of 153.6 particles/m^2, i.e., approximately 40 particles per element.

3.2. ERT Data

The synthetic model is completed by assuming that four boreholes are available, each equipped with 16 electrodes, for a 2-D time-lapse ERT acquisition. The borehole electrodes are 1 m vertically spaced and connected to an additional line of surface electrodes (also 1 m spaced), forming a surface/cross-borehole configuration with a total of 91 electrodes. ERT data are collected every 60 h, from $t = 60$ h to $t = 480$ h, for a total of eight observation vectors available for assimilation.

In order to map values of concentration C into bulk electrical conductivity σ, we applied Archie's law (4) for fully saturated media, with a porosity ϕ equal to 30% and a cementation exponent $m = 1.3$. We decided not to introduce uncertainty with respect to the Archie's law parameters because we wanted to compare the performance of the proposed approaches highlighting their essential features, with no interference of other uncertainty issues. It must be noted that the information content of the data lies practically only in the tracer travel times. Given that for any value of the cementation index the relationship between bulk electrical conductivity and water electrical conductivity is always monotonic, an exact knowledge of the cementation index value has practically no influence on the determination of the tracer travel time, and thus it bears little to no consequence in the data assimilation procedure here discussed. Water electrical conductivity σ_w in equation (4) is obtained from concentrations C assuming that the maximum dimensionless concentration corresponds to the maximum dimensional concentration of 6 g/L, considered to be the maximum solute concentration for which gravimetric sinking is not observed [*Kemna et al.*, 2002; *Cassiani et al.*, 2006; *Monego et al.*, 2010; *Perri et al.*, 2012]. We further assume that the dissolved solute is NaCl, and we use the relationship between molar concentration and water electrical conductivity established by *Sambuelli and Comina* [2010] and partially based on the theoretical derivation by *Atkins and de Paula* [2006].

Figure 3 reports, for both the isotropic and anisotropic reference fields, a snapshot of the solute concentration at the end of the experiment, after 480 h from the injection, along with the corresponding electrical resistivity tomography. Despite some oversmoothing, which is typical of electrical inversions obtained with methods such as the one described in section 2.2, the data capture well the dynamics of the saline tracer. Electrical conductivity data such as those shown in the figure are assimilated in the uncoupled approach, while the fully coupled approach uses the raw resistance data that were used to obtain the ERT images.

In order for the coupled approach to be consistent with the uncoupled, the same error value has been assigned to the resistance data. Therefore, in the coupled approach, the diagonal elements in $\mathbf{R}_e$ were

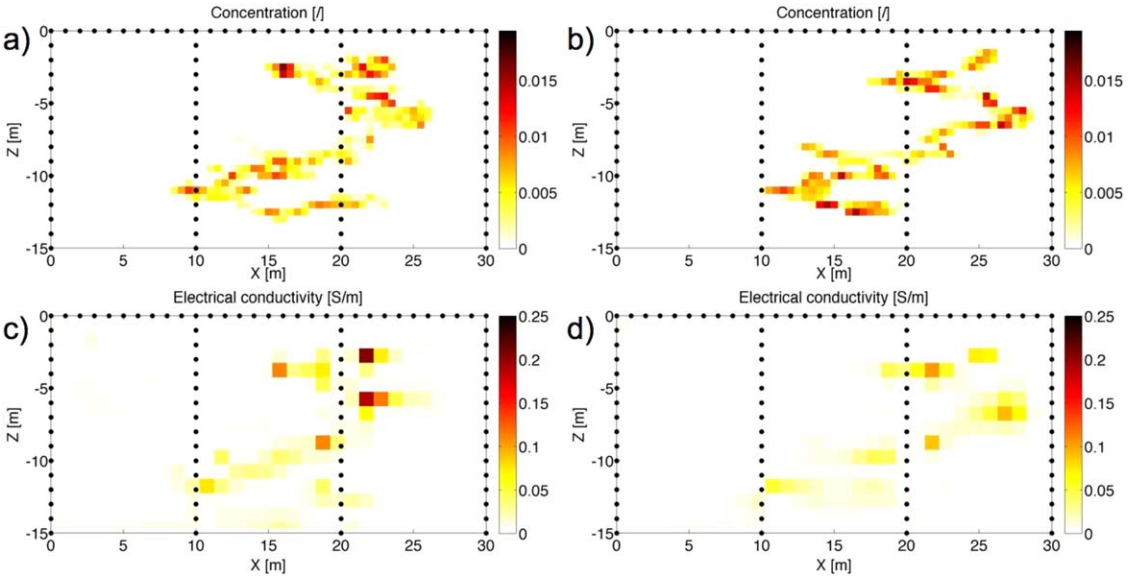

Figure 3. Solute concentration (dimensionless) in the (a) isotropic and (b) anisotropic reference fields, along with (c, d) the corresponding electrical conductivity (S/m) distributions obtained at time $t = 480$ h by the hydrogeophysical inversion described in section 2.2.

computed by assigning a standard deviation of 2% of the observed resistance data and the off-diagonal elements were set to zero. Consistently, the electrical inversions used in the uncoupled approach were run to a goal of 2% error.

3.3. Inversion Results

For each reference field, we tested the two inverse approaches in six scenarios, where the prior ensemble of hydraulic log-conductivity distributions was generated by using geostatistical parameters intentionally different from the ones used to generate the true hydraulic conductivity field. The scenarios are summarized in Table 1. In scenario 1 the prior ensemble of Y fields was generated with an overestimated variance, in scenario 2 with a biased mean and overestimated variance, in scenarios 3 and 4 with wrong prior correlation lengths, and in scenarios 5 and 6 all the above errors are combined.

A preliminary sensitivity analysis showed that increasing the ensemble size from 2500 to 5000 did not improve significantly the performance of the inversion; therefore, an ensemble size of $NMC = 2500$ was used for all the scenarios. Such ensemble size is very large compared to applications of EnKF for the estimation of homogeneous parameters, where it typically does not exceed $O(10^2)$. However, in this case the problem is characterized by a large number of unknowns (specifically 1800); therefore, a large number of realizations is needed to sufficiently explore the whole range of Y variability.

3.3.1. Isotropic Scenarios

Table 2 summarizes the results of all the isotropic scenarios in terms of average absolute error of the retrieved hydraulic conductivity fields (AAE_Y) and concentration distributions (AAE_C) computed "ex post" by running the transport model using the retrieved K fields. The errors are computed as

Table 1. Prior Statistics of Investigated Scenarios

	Isotropic				Anisotropic			
Scenario	$\langle Y \rangle$	σ_Y^2	I_x	I_z	$\langle Y \rangle$	σ_Y^2	I_x	I_z
Reference	0.0	1.0	1.0	1.0	0.0	1.0	4.0	1.0
1	0.0	1.5	1.0	1.0	0.0	1.5	4.0	1.0
2	−0.5	1.5	1.0	1.0	−0.5	1.5	4.0	1.0
3	0.0	1.0	2.0	2.0	0.0	1.0	8.0	2.0
4	0.0	1.0	0.5	0.5	0.0	1.0	2.0	0.5
5	−0.5	1.5	2.0	2.0	−0.5	1.5	8.0	2.0
6	−0.5	1.5	0.5	0.5	−0.5	1.5	2.0	0.5

Table 2. Performance of the Isotropic Scenarios in Terms of Average Absolute Error of the Retrieved Hydraulic Log Conductivity Fields and Concentration Distributions Computed With "Ex Post" Simulations Run in the Inverted *Y* Fields[a]

	Coupled		Uncoupled		Open Loop	
Scenario	AAE_Y	AAE_C	AAE_Y	AAE_C	AAE_Y	AAE_C
1	0.39	0.00057	0.50	0.00076	0.52	0.00094
2	0.48	0.00058	0.48	0.00070	0.56	0.00101
3	0.45	0.00060	0.44	0.00073	0.36	0.00095
4	0.39	0.00052	0.47	0.00069	0.47	0.00089
5	0.87	0.00078	0.47	0.00071	0.44	0.00103
6	0.72	0.00079	0.53	0.00071	0.56	0.00099

[a]Open loop (i.e., simulations with prior *Y* fields) results are reported for comparison.

$$AAE_Y = \frac{1}{NMC}\frac{1}{n}\sum_{i=1}^{NMC}\sum_{j=1}^{n}|Y_j^i - Y_j^{true}|,$$
$$AAE_C = \frac{1}{NMC}\frac{1}{n}\sum_{i=1}^{NMC}\sum_{j=1}^{n}|C_j^i - C_j^{true}|, \quad (9)$$

where *NMC* is the number of realizations and *n* is the number of elements, i.e., the number of *Y* and *C* values to estimate. The table also reports the "open loop" results, i.e., the AAE_Y and AAE_C computed using the prior ensemble of hydraulic log-conductivity fields.

First of all, it can be noted that in all scenarios both inversion methods provide significant improvements with respect to the open loop. Even when the AAE_Y of the inverted field is larger than the one of the open

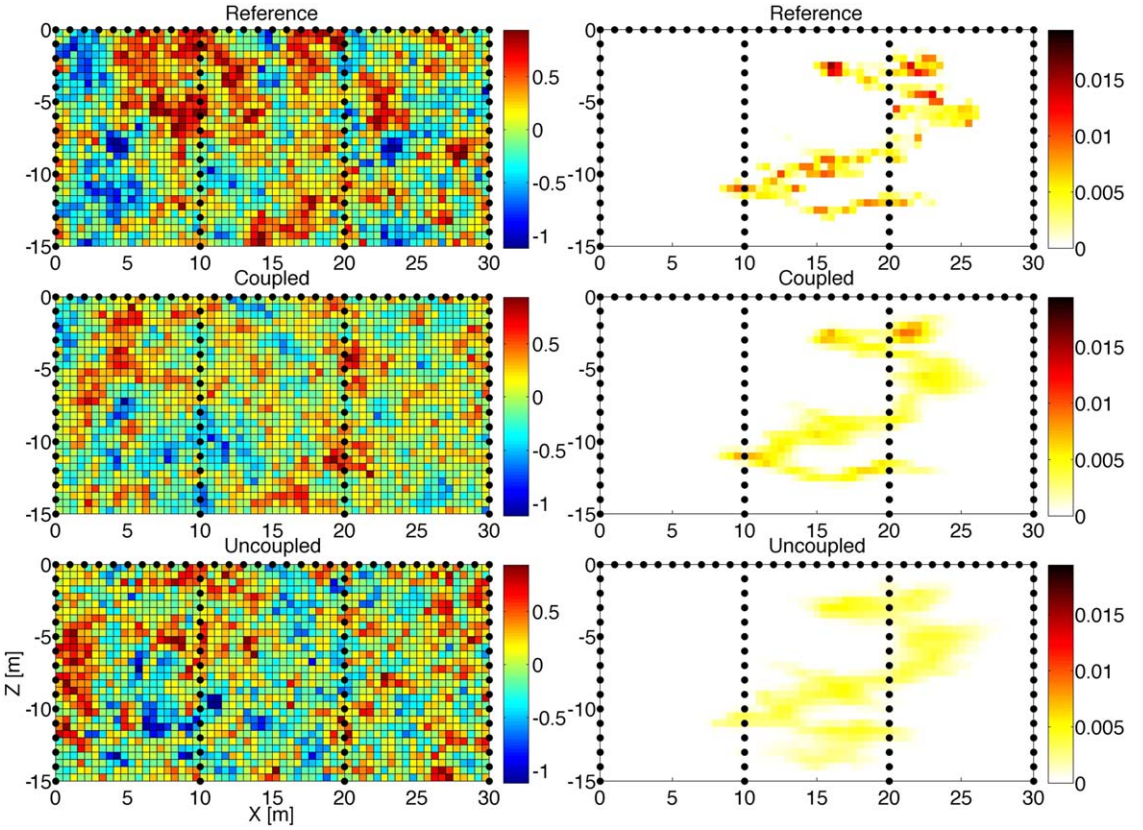

Figure 4. (top) Reference *Y* distribution and corresponding saline tracer concentration at $t = 480$ h; (middle) *Y* distribution estimated in scenario 4 by the coupled inversion and corresponding saline tracer concentration at $t = 480$ h; (bottom) *Y* distribution estimated in scenario 4 by the uncoupled inversion and corresponding saline tracer concentration at $t = 480$ h. The fields in the middle and bottom row figures are ensemble means over 2500 realizations. Color bars on the left and right indicate hydraulic log-conductivity in $\log_{10}$[m/h] and dimensionless concentration, respectively.

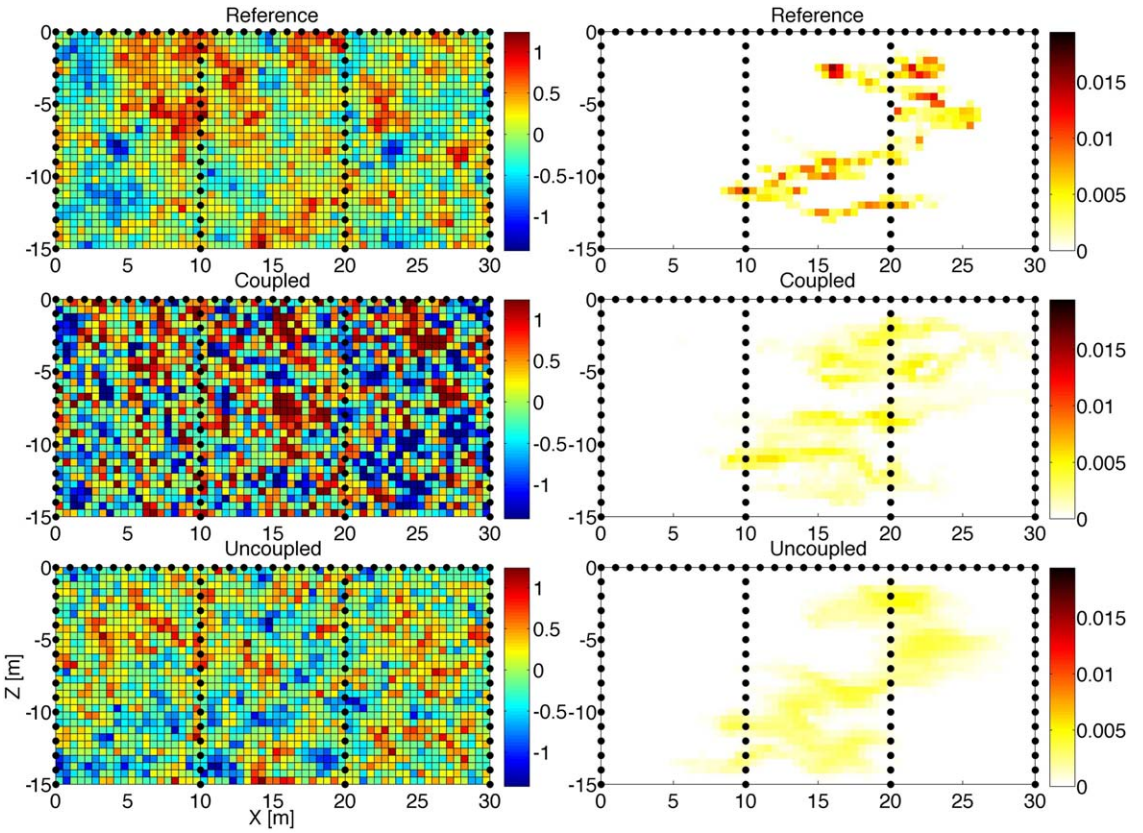

Figure 5. (top) Reference *Y* distribution and corresponding saline tracer concentration at $t = 480$ h; (middle) *Y* distribution estimated in scenario 6 by the coupled inversion and corresponding saline tracer concentration at $t = 480$ h; (bottom) *Y* distribution estimated in scenario 6 by the uncoupled inversion and corresponding saline tracer concentration at $t = 480$ h. The fields in the middle and bottom row figures are ensemble means over 2500 realizations. Color bars on the left and right indicate hydraulic log-conductivity in $\log_{10}$[m/h] and dimensionless concentration, respectively.

loop, the values of AAE_C show that the tracer evolution is better reproduced using the updated *Y* distributions. Regarding the comparison between the two methods, on one hand, the coupled approach performs better than the uncoupled one when the geostatistical parameters are close to the true ones, i.e., in scenarios 1–4. For instance, even in scenario 3, where AAE_Y of the coupled inversion is slightly larger than in the uncoupled one (0.45 versus 0.44), the concentration distribution at the end of the simulated period is reproduced much better by the *Y* field estimated with the fully coupled approach (6.0×10^{-4} versus 7.3×10^{-4}). On the other hand, results of scenarios 5 and 6 show that while the uncoupled approach performs consistently with scenarios 1–4, the coupled approach is subject to an apparent deterioration of the final solution, in terms of both hydraulic conductivity and tracer concentration.

The reason for this behavior can be explained by looking in more detail at the inversion results. For brevity, we show detailed results of only two scenarios (4 and 6), which are nevertheless representative of the general behavior of the two inverse approaches.

In scenario 4, where prior mean and variance are correct, but correlation length is underestimated, both the coupled and uncoupled inversions obtain a good representation of the true hydraulic conductivity field, as can be seen in Figure 4. In particular, the coupled approach outperforms the uncoupled one in the prediction of the saline tracer plume, which in the uncoupled approach is affected by more uncertainty, as a result of the oversmoothing affecting the assimilated data.

In scenario 6 (Figure 5), where the prior ensemble is generated with a biased mean, the coupled approach fails to recover the true field and, as a consequence, the concentration distribution, while the uncoupled approach performs better, even though with the same uncertainty and oversmoothing effects observed in the previous scenarios.

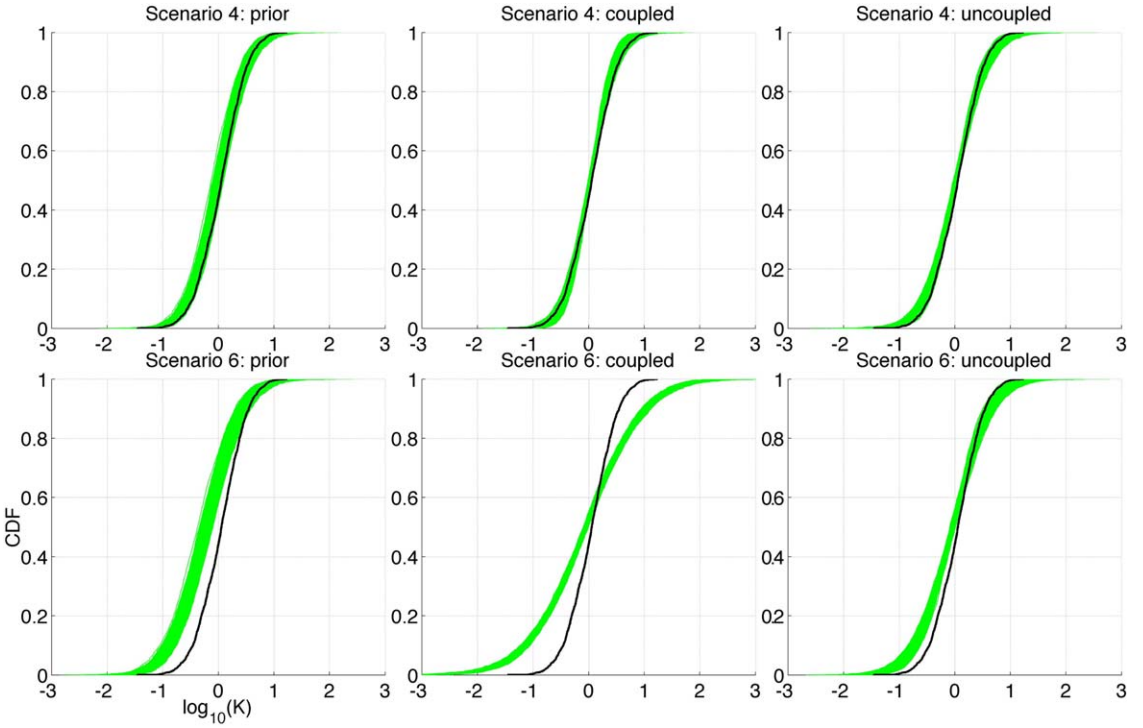

Figure 6. Cumulative distribution function (CDF) of the prior ensemble of *Y* fields, the final ensemble of retrieved *Y* fields in the coupled approach, and the final ensemble of retrieved *Y* fields in the uncoupled approach for (top) scenario 4 and (bottom) scenario 6. Green lines indicate the CDF ensembles, while the black lines denote the true *Y* CDF.

The results can also be investigated by comparing the cumulative distribution functions (CDFs) of the hydraulic log-conductivity for the prior and the final ensembles, reported in Figure 6, with the CDF of the reference *Y* field. In scenario 4, despite the underestimated correlation length, the prior ensemble, which is the same for the two approaches, incorporates the variability of the true field; for this reason, the coupled approach rapidly reduces the uncertainty around the true solution, due to the small uncertainty of the resistance measurements. The uncoupled approach is affected by the larger uncertainty of the electrical conductivity observations; as a result, more uncertainty affects the tails of the estimated distribution and this is finally reflected on the prediction of the tracer plume. The median instead is captured with a small uncertainty in both cases.

In scenario 6, in contrast, the initial hydraulic log-conductivity ensemble does not incorporate the variability of the true field. The coupled approach, being characterized by a high confidence on the measurements, i.e., small observation errors, reduces too quickly the uncertainty of the ensemble around the wrong solution. This is a manifestation of the filter divergence or inbreeding [*Hendricks Franssen and Kinzelbach*, 2008; *Evensen*, 2009], which is an effect of variance reduction usually caused by sampling errors resulting from the use of a finite ensemble. These sampling errors are seen as spurious correlations over long spatial distances or between variables that are supposed to be uncorrelated, leading to small unphysical updates of the variables in each ensemble member, and eventually to a strongly underestimated variance. In this case, the filter inbreeding occurs early in the simulation and further assimilations have no physical meaning, gradually leading to the divergence of the inverted *Y* field. This effect is prevented in the uncoupled case, due to the larger uncertainty of the assimilated measurements. The uncoupled approach is thus able to gradually adjust the solution, as evidenced by the better approximation of the distribution tails. Again, the median tends to be correctly matched by both approaches.

3.3.2. Anisotropic Scenarios

Table 3 summarizes the performance of the anisotropic scenarios. The results are broadly consistent with those of the isotropic runs: except for the coupled approach in scenario 6, all the inverted hydraulic log-conductivity fields show an improved description of the saline tracer evolution compared with the prior *Y*

Table 3. Performance of the Anisotropic Scenarios in Terms of Average Absolute Error of the Retrieved Hydraulic Log Conductivity Fields and Concentration Distributions Computed With "Ex Post" Simulations Run in the Inverted *Y* Fields[a]

	Coupled		Uncoupled		Open loop	
Scenario	AAE_Y	AAE_C	AAE_Y	AAE_C	AAE_Y	AAE_C
1	0.17	0.00039	0.23	0.00066	0.26	0.00095
2	0.35	0.00066	0.22	0.00072	0.35	0.00102
3	0.48	0.00086	0.28	0.00077	0.18	0.00097
4	0.17	0.00038	0.22	0.00068	0.23	0.00094
5	0.54	0.00078	0.25	0.00084	0.30	0.00104
6	1.99	0.00111	0.26	0.00067	0.35	0.00101

[a]Open loop (i.e., simulations with prior *Y* fields) results are reported for comparison.

distributions. The coupled approach performs better than the uncoupled one, both in terms of hydraulic conductivity and concentrations, in scenarios 1 and 4, where the prior mean $\langle Y \rangle$ is correct. In scenarios 2 and 5, despite a larger AAE_Y, the tracer dynamics is still better captured by the coupled method, whereas in scenarios 3 and 6 the uncoupled approach provides the best results. In particular, the combination of wrong prior mean and underestimated correlation lengths (scenario 6) leads to the divergence of the coupled method with AAE_C and, especially, AAE_Y values much larger than in the open loop.

These results confirm that the coupled method is more prone to the filter inbreeding than the uncoupled one and lead to the question on whether the coupled approach can benefit more than the uncoupled one from the use of some countermeasures. We then rerun the anisotropic scenario 6, the most affected, with both the coupled and uncoupled approaches, using covariance inflation with a constant inflation factor equal to 1.01 [*Evensen*, 2009]. The results of this analysis are shown in Figure 7 in terms of AAE_Y. It is clear how the coupled method is affected by the filter divergence when no inflation is used, as evidenced by the progressive increase of the error and by the fact that after $t = 360$ h no further updates are performed by EnKF, sign that the system state error covariance matrix collapsed to zero. The use of covariance inflation significantly improves the performance of the coupled approach, with a final value of AAE_Y much smaller than in the case without inflation. However, the performance of the coupled approach is still poorer than the one of the uncoupled method, which is not affected by the inflation and in both cases exhibits a constantly decreasing AAE_Y. Analogous conclusions can be drawn from the analysis of the AAE_C behavior (not shown). This is a further confirmation of the robustness of the uncoupled inversion approach.

3.4. Numerical Performance

A detailed investigation about the numerical performance of the two inversion methods was not carried out, as different computers were used for the various scenarios. However, an approximate analysis of the computational effort required by the two methods reveals that the fully coupled approach needs about 10 times as much CPU time as the uncoupled approach. In both cases, the main fraction of the total CPU time is required by the forward electrical model, but the uncoupled approach requires much fewer calls (approximately 2.5×10^5, including the computation of $\mathbf{R}_e$) than the fully coupled, which needs a forward electrical model run for each electrode, realization, and time step (i.e., approximately 1.8×10^6 in this application).

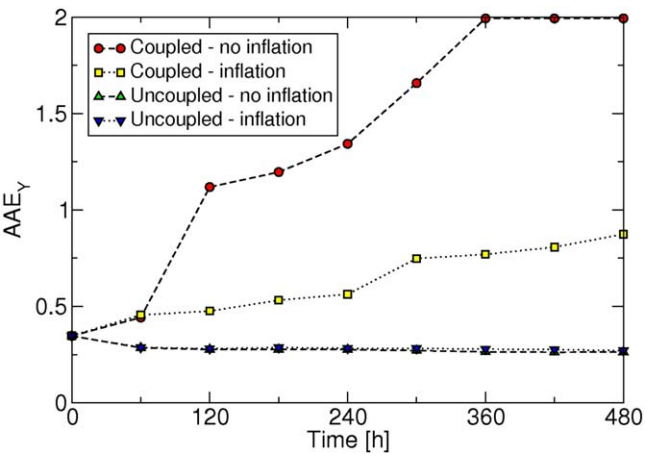

Figure 7. Average absolute error of the hydraulic log-conductivity fields obtained in the coupled and uncoupled anisotropic scenario 6 with and without covariance inflation.

4. Discussion and Conclusions

We carried out a comparison analysis between a coupled and an uncoupled approach for hydrogeophysical inverse modeling based on the

assimilation via ensemble Kalman filter (EnKF) of electrical resistivity tomography (ERT) data into a Lagrangian model of groundwater transport. The two approaches were evaluated in terms of their capability of retrieving the hydraulic conductivity (K) spatial distribution of two synthetic heterogeneous aquifers, one isotropic and one anisotropic, in a number of scenarios where the assumed prior geostatistical parameters deviate from the reference.

The results show that the coupled approach outperforms the uncoupled one when the prior geostatistical parameters are close to the true ones. This happens because the coupled approach (i) is not affected by overdispersion resulting from the regularization term typically used in electrical inversions and (ii) gives more confidence to the measurements than the uncoupled method does, due to the smaller errors affecting the raw resistance data compared with the uncertainty associated to the electrical images. However, lack of regularization and overconfidence in the measurements can become a problem when the initial ensemble of K distributions is biased: in this case the coupled approach is heavily affected by filter inbreeding, an undesired effect of variance reduction typical of EnKF applications, and, as a consequence, fails to retrieve the reference K field.

The issue of filter divergence in the uncoupled approach is significantly alleviated by the larger uncertainty on the observations and the measurement error correlation terms (off-diagonal elements in matrix $\mathbf{R}_e$) resulting from the previous electrical inversion. For this reason, the uncoupled approach is more robust than the coupled one with respect to prior information on the initial ensemble, despite the presence of overdispersion due to the regularization used in the preliminary electrical inversion. The use of covariance inflation, one of the most common countermeasures to reduce or prevent filter inbreeding, in the scenario where the coupled approach performed worst, improved the inversion performance. However, the uncoupled approach, which proved to be insensitive to the inflation, still outperformed the coupled one.

Overall, it seems that the coupled approach is more affected by the problem of filter inbreeding due to a combined effect of overconfidence on the assimilated raw data and the absence of a "preprocessing" step like the one represented by the preliminary geophysical inversion in the uncoupled scheme. In other words, filter inbreeding is probably a manifestation of the fact that in the coupled approach the assumed error level is smaller than it should be. At a first glance this seems to be a self-contradiction. As in the coupled approach we use the resistance data per se, we reasonably assumed for the error level the same value used in the geophysical inversion embedded in the uncoupled approach. Along the same line of reasoning we also deemed acceptable the assumption of resistance measurement errors independent of each other, i.e., the assumption of a diagonal observation error matrix. However, on second thought, it would be reasonable to expect that the errors affecting measured resistances are indeed correlated through the structure of the resistivity distribution itself, which however is unknown at the stage where errors need to be estimated. This error correlation is instead explicitly computed, using a standard approach, in the electrical inversion used in the uncoupled approach, whereby the correlation between estimated resistivities is assessed given the resistance values. Symmetrically, in the coupled approach, one should compute the correlation between the measured resistances given the underlying resistivity distribution, a task that would require further theoretical developments, warranting a study on its own.

Based on the results of this study, we argue that the relative merit of the coupled approach versus the uncoupled one cannot be assumed a priori and should be assessed case by case. As the information content of the geophysical data remains the same in both the coupled and uncoupled methods, the main difference is the approach taken in order to complement the information content and construct an "image" of the process. In the uncoupled approach the regularization is given by smoothness constraints, while in the coupled approach a sort of regularization is provided by the hydrological model itself, which may be as erroneous (e.g., errors in modeling conceptualization, boundary conditions, etc.) as assuming that the resistivity distribution is smooth. It is in fact true that the uncoupled approach may be adversely affected by artifacts caused by geophysical inversion—the most common being the well-known mass balance problems—but in some cases the artifacts do not (or only slightly) impact the information content of the inverted images. This is the case of the tracer tests in the saturated zone discussed in this paper, where the information is mainly contained in the travel time of the tracer and not in its overall mass. For other cases the uncoupled approach may indeed suffer more, e.g., in the case of infiltration in the unsaturated zone, where mass balance issues are of utmost importance [e.g., *Manoli et al*., 2015]. On the other hand, it may be argued that the coupled approach may be more risky, as strong unjustified assumptions can be made on the nature

of the transport process and thus on its modeling approach. Although this is not the case in this study, where modeling is conceptually correct (being it all a synthetic exercise), the assumption of prior information too far from the reference *K* field ultimately results in a coupled inversion scheme that, relying exclusively on the capability of the EnKF with underestimated measurement errors, is too rigidly constrained and thus unable to correct initial deviations of the prior guess from the true solution.

In light of the above discussion, and given that the uncoupled approach requires a small computational effort (about 1/10 of CPU time) compared to the coupled one, we conclude that running both types of inversion is recommended in most cases (if the total computational cost is still affordable). As the uncoupled approach is more robust but also more uncertain, it may be used as a preliminary inversion before refining the results with a fully coupled approach. It may also give a good indication on whether the results from the corresponding coupled inversion are reliable or are affected by numerical artifacts due to filter inbreeding. Once sufficiently accurate prior information has been obtained, coupled approaches have the undoubted advantage that the numerical models for the geophysical and hydrological processes are linked together such that the geophysical data are inverted directly for the hydrological properties of interest, avoiding artifacts related to more traditional geophysical inversions.

Note that although the conclusions of this study are strictly applicable only to the inversion tool we used, i.e., the ensemble Kalman filter, analogous issues related to the definition of the measurement uncertainty level might affect other methods of coupled inversions, potentially manifesting themselves in different ways. For this reason we urge similar comparison studies to be carried out with other inversion methods, in order to further advance our knowledge on hydrogeophysical inversions.

Acknowledgments
This work was supported by the University of Padua (project CPDA115351/11 "Identification of hydraulic parameters in sedimentary aquifers at the local and catchment scales"). We thank the Associate Editor and three anonymous reviewers for their constructive remarks that helped to improve the quality of the paper. The synthetic data used in this study are available from the corresponding author upon request.

References

Annan, A. P. (2005), GPR methods for hydrogeological studies, in *Hydrogeophysics*, edited by Y. Rubin, and S. S. Hubbard, vol. 50, pp. 185–213, Springer, Dordrecht, Netherlands.

Archie, G. E. (1942), The electrical resistivity log as an aid in determining some reservoir characteristics, *Pet. Technol.*, *1*, 55–62.

Atkins, P., and J. de Paula (2006), *Physical Chemistry*, Oxford Univ. Press, Oxford, U. K.

Binley, A. M., and A. Kemna (2005), Electrical methods, in *Hydrogeophysics*, edited by Y. Rubin, and S. S. Hubbard, vol. 50, pp. 129–156, Springer, Dordrecht, Netherlands.

Busch, S., L. Weihermüller, J. A. Huisman, C. M. Steelman, A. L. Endres, H. Vereecken, and J. van der Kruk (2013), Coupled hydrogeophysical inversion of time-lapse surface GPR data to estimate hydraulic properties of a layered subsurface, *Water Resour. Res.*, *49*, 8480–8494, doi:10.1002/2013WR013992.

Camporese, M., C. Paniconi, M. Putti, and P. Salandin (2009a), Ensemble Kalman filter data assimilation for a process-based catchment scale model of surface and subsurface flow, *Water Resour. Res.*, *45*, W10421, doi:10.1029/2008WR007031.

Camporese, M., C. Paniconi, M. Putti, and P. Salandin (2009b), Comparison of data assimilation techniques for a coupled model of surface and subsurface flow, *Vadose Zone J.*, *8*(4), 837–845, doi:10.2136/vzj2009.0018.

Camporese, M., G. Cassiani, R. Deiana, and P. Salandin (2011), Assessment of local hydraulic properties from electrical resistivity tomography monitoring of a three-dimensional synthetic tracer test experiment, *Water Resour. Res.*, *47*, W12508, doi:10.1029/2011WR010528.

Carrera, J., and S. P. Neuman (1986), Estimation of aquifer parameters under transient and steady-state conditions: 1. Maximum-likelihood method incorporating prior information, *Water Resour. Res.*, *22*(2), 199–210, doi:10.1029/WR022i002p00199.

Carrera, J., A. Medina, and G. Galarza (1993), Groundwater inverse problem: Discussion on geostatistical formulations and validation, *Hydrogeologie*, *4*, 313–324.

Cassiani, G., V. Bruno, A. Villa, N. Fusi, and A. M. Binley (2006), A saline tracer test monitored via time-lapse surface electrical resistivity tomography, *J. Appl. Geophys.*, *59*, 244–259.

Cassiani, G., et al. (2012), Noninvasive monitoring of soil static characteristics and dynamic states: A case study highlighting vegetation effects on agricultural land, *Vadose Zone J.*, *11*(3), doi:10.2136/vzj2011.0195.

Certes, C., and G. De Marsily (1991), Application of the pilot point method to the identification of aquifer transmissivities, *Adv. Water Resour.*, *14*, 284–300, doi:10.1016/0309-1708(91)90040-U.

Chen, Y., and D. Zhang (2006), Data assimilation for transient flow in geologic formations via ensemble Kalman filter, *Adv. Water Resour.*, *29*, 1107–1122, doi:10.1016/j.advwatres.2005.09.007.

Cordes, C., and W. Kinzelbach (1992), Continuous groundwater velocity-fields and path lines in linear, bilinear, and trilinear finite-elements, *Water Resour. Res.*, *28*(11), 2903–2911, doi:10.1029/92WR01686.

Crestani, E., M. Camporese, D. Baú, and P. Salandin (2013), Ensemble Kalman filter versus ensemble smoother for assessing hydraulic conductivity via tracer test data assimilation, *Hydrol. Earth Syst. Sci.*, *17*, 1517–1531, doi:10.5194/hess-17-1517-2013.

Dagan, G. (1989), *Flow and Transport in Porous Formations*, Springer, Berlin.

Day-Lewis, F. D., K. Singha, and A. M. Binley (2005), The application of petrophysical models to radar and electrical resistivity tomograms: Resolution dependent limitations, *J. Geophys. Res.*, *110*, B08206, doi:10.1029/2004JB003569.

Deiana, R., G. Cassiani, A. Villa, A. Bagliani, and V. Bruno (2008), Calibration of a vadose zone model using water injection monitored by GPR and electrical resistance tomography, *Vadose Zone J.*, *7*(1), 215–226, doi:10.2136/vzj2006.0137.

Evensen, G. (2009), The ensemble Kalman filter for combined state and parameter estimation, *IEEE Control Syst. Mag.*, *29*(3), 83–104, doi:10.1109/MCS.2009.932223.

Gelhar, L. (1993), *Stochastic Subsurface Hydrology*, Prentice Hall, Upper Saddle River, N. J.

Gomez-Hernandez, J., A. Sahuquillo, and J. Capilla (1997), Stochastic simulation of transmissivity fields conditional to both transmissivity and piezometric data—I. Theory, *J. Hydrol.*, *203*, 162–174.

Gutjahr, A., B. Bullard, and S. Hatch (1997), General joint conditional simulations using a fast Fourier transform method, *Math. Geol.*, *29*(3), 361–389, doi:10.1007/BF02769641.
Hendricks Franssen, H. J., and W. Kinzelbach (2008), Real-time groundwater flow modeling with the Ensemble Kalman Filter: Joint estimation of states and parameters and the filter inbreeding problem, *Water Resour. Res.*, *44*, W09408, doi:10.1029/2007WR006505.
Hendricks Franssen, H. J., and W. Kinzelbach (2009), Ensemble Kalman filtering versus sequential self-calibration for inverse modelling of dynamic groundwater flow systems, *J. Hydrol.*, *365*, 261–274, doi:10.1016/j.jhydrol.2008.11.033.
Hinnell, A. C., T. P. A. Ferré, J. A. Vrugt, J. A. Huisman, S. Moysey, J. Rings, and M. B. Kowalsky (2010), Improved extraction of hydrologic information from geophysical data through coupled hydrogeophysical inversion, *Water Resour. Res.*, *46*, W00D40, doi:10.1029/2008WR007060.
Irving, J., and K. Singha (2010), Stochastic inversion of tracer test and electrical geophysical data to estimate hydraulic conductivities, *Water Resour. Res.*, *46*, W11514, doi:10.1029/2009WR008340.
Jardani, A., A. Revil, and J. P. Dupont (2013), Stochastic joint inversion of hydrogeophysical data for salt tracer test monitoring and hydraulic conductivity imaging, *Adv. Water Resour.*, *52*, 62–77, doi:10.1016/j.advwatres.2012.08.005.
Judd, K., and T. Stemler (2010), Forecasting: It is not about statistics, it is about dynamics, *Philos. Trans. R. Soc. A*, *386*(1910), 263–271, doi:10.1098/rsta.2009.0195.
Karahan, H., and M. Ayvaz (2008), Simultaneous parameter identification of a heterogeneous aquifer system using artificial neural networks, *Hydrogeol. J.*, *16*(5), 817–827, doi:10.1007/s10040-008-0279-0.
Kemna, A., J. Vanderborght, B. Kulessa, and H. Vereecken (2002), Imaging and characterisation of subsurface solute transport using electrical resistivity tomography (ERT) and equivalent transport models, *J. Hydrol.*, *267*, 125–146, doi:10.1016/S0022-1694(02)00145-2.
Li, L., H. Zhou, J. J. Gomez-Hernandez, and H. J. Hendricks Franssen (2012), Jointly mapping hydraulic conductivity and porosity by assimilating concentration data via ensemble Kalman filter, *J. Hydrol.*, *428*, 152–169, doi:10.1016/j.jhydrol.2012.01.037.
Manoli, G., M. Rossi, D. Pasetto, R. Deiana, S. Ferraris, G. Cassiani, and M. Putti (2015), An iterative particle filter approach for coupled hydrogeophysical inversion of a controlled infiltration experiment, *J. Comput. Phys.*, *283*, 37–51, doi:10.1016/j.jcp.2014.11.035.
Margulis, S. A., D. McLaughlin, D. Entekhabi, and S. Dunne (2002), Land data assimilation and estimation of soil moisture using measurements from the Southern Great Plains 1997 field experiment, *Water Resour. Res.*, *38*(12), 1299, doi:10.1029/2001WR001114.
McLaughlin, D., and L. R. Townley (1996), A reassessment of the groundwater inverse problem, *Water Resour. Res.*, *32*(5), 1131–1161, doi:10.1029/96WR00160.
Menke, W. (1984), The resolving power of cross-borehole tomography, *Geophys. Res. Lett.*, *11*(2), 105–108.
Monego, M., G. Cassiani, R. Deiana, M. Putti, G. Passadore, and L. Altissimo (2010), Tracer test in a shallow heterogeneous aquifer monitored via time-lapse surface ERT, *Geophysics*, *75*(4), WA61–WA73, doi:10.1190/1.3474601.
Montzka, C., V. R. N. Pauwels, H. J. Hendricks Franssen, X. J. Han, and H. Vereecken (2012), Multivariate and multiscale data assimilation in terrestrial systems: A review, *Sensors*, *12*(12), 16,291–16,333, doi:10.3390/s121216291.
Pauwels, V. R. N., R. Hoeben, N. E. C. Verhoest, and F. P. De Troch (2001), The importance of the spatial patterns of remotely sensed soil moisture in the improvement of discharge predictions for small-scale basins through data assimilation, *J. Hydrol.*, *251*(1–2), 88–102, doi:10.1016/S0022-1694(01)00440-1.
Perri, M. T., G. Cassiani, I. Gervasio, R. Deiana, and A. M. Binley (2012), A saline tracer test monitored via both surface and cross-borehole electrical resistivity tomography: Comparison of time-lapse results, *J. Appl. Geophys.*, *79*, 6–16.
Pollock, D., and O. Cirpka (2010), Fully coupled hydrogeophysical inversion of synthetic salt tracer experiments, *Water Resour. Res.*, *46*, W07501, doi:10.1029/2009WR008575.
RamaRao, B., A. Lavenue, G. De Marsily, and M. Marietta (1995), Pilot point methodology for automated calibration of an ensemble of conditionally simulated transmissivity fields: 1. Theory and computational experiments, *Water Resour. Res.*, *31*(3), 475–493, doi:10.1029/94WR02258.
Sakov, P., G. Evensen, and L. Bertino (2010), Asynchronous data assimilation with the EnKF, *Tellus, Ser. A*, *62*(1), 24–29, doi:10.1111/j.1600-0870.2009.00417.x.
Salandin, P., and V. Fiorotto (1998), Solute transport in highly heterogeneous aquifers, *Water Resour. Res.*, *34*(5), 949–961, doi:10.1029/98WR00219.
Sambuelli, L., and C. Comina (2010), Fast ERT to estimate pollutants and solid transport variation in water flow: A laboratory experiment, *Boll. Geofis. Teor. Appl.*, *51*(1), 1–22.
Singha, K., and S. Gorelick (2005), Saline tracer visualized with three-dimensional electrical resistivity tomography: Field-scale spatial moment analysis, *Water Resour. Res.*, *41*, W05023, doi:10.1029/2004WR003460.
Singha, K., F. D. Day-Lewis, T. Johnson, and L. D. Slater (2015), Advances in interpretation of subsurface processes with time-lapse electrical imaging, *Hydrol. Processes*, *29*, 1549–1576, doi:10.1002/hyp.10280.
Soueid Ahmed, A., A. Jardani, A. Revil, and J. P. Dupont (2014), Hydraulic conductivity field characterization from the joint inversion of hydraulic heads and self-potential data, *Water Resour. Res.*, *50*, 3502–3522, doi:10.1002/2013WR014645.
Tran, A. P., M. Vanclooster, M. Zupanski, and S. Lambot (2014), Joint estimation of soil moisture profile and hydraulic parameters by ground-penetrating radar data assimilation with maximum likelihood ensemble filter, *Water Resour. Res.*, *50*, 3131–3146, doi:10.1002/2013WR014583.
Vereecken, H., A. Binley, G. Cassiani, A. Revil, and K. Titov (Eds.) (2006), *Applied Hydrogeophysics, Nato Sci. Ser. IV*, vol. 71, Springer, Dordrecht, Netherlands.
Vrugt, J. A., P. H. Stauffer, T. Wöhling, B. A. Robinson, and V. V. Vesselinov (2008), Inverse modeling of subsurface flow and transport properties: A review with new developments, *Vadose Zone J.*, *7*, 843–864, doi:10.2136/vzj2007.0078.
Wen, X.-H., and W. H. Chen (2006), Real-time reservoir model updating using ensemble Kalman filter with confirming option, *SPEJ Soc. Pet. Eng. J.*, *11*, 431–442, doi:10.2118/92991-PA.
Xu, T., J. J. Gómez-Hernández, H. Zhou, and L. Li (2013), The power of transient piezometric head data in inverse modeling: An application of the localized normal-score EnKF with covariance inflation in a heterogenous bimodal hydraulic conductivity field, *Adv. Water Resour.*, *54*, 100–118, doi:10.1016/j.advwatres.2013.01.006.
Zhou, H., J. J. Gómez-Hernández, and L. Li (2014), Inverse methods in hydrogeology: Evolution and recent trends, *Adv. Water Resour.*, *63*, 22–37, doi:10.1016/j.advwatres.2013.10.014.
Zimmerman, D. A., et al. (1998), A comparison of seven geostatistically based inverse approaches to estimate transmissivities for modeling advective transport by groundwater flow, *Water Resour. Res.*, *34*(6), 1373–1413, doi:10.1029/98WR00003.